4538 *Biochemistry* **2009,** *48,* 4538–4547
DOI:10.1021/bi802359b

BIOCHEMISTRY
including biophysical chemistry & molecular biology
*Article*

# Transition State Structures and the Roles of Catalytic Residues in GAP-Facilitated GTPase of Ras As Elucidated by $^{18}O$ Kinetic Isotope Effects†

Xinlin Du* and Stephen R. Sprang‡

*Department of Biochemistry, University of Texas, Southwestern Medical Center, 6001 Forest Park, Room ND10.300, Dallas, Texas 75390-9050 ‡ Current address: Center for Biomolecular Structure and Dynamics, University of Montana, 32 Campus Drive, Missoula, MT 59812.*

*Received December 25, 2008; Revised Manuscript Received April 6, 2009*

ABSTRACT: Ras-catalyzed guanosine 5′ triphosphate (GTP) hydrolysis proceeds through a loose transition state as suggested in our previous study of $^{18}O$ kinetic isotope effects (KIE) [Du, X. et al. ((2004) ) *Proc. Natl. Acad. Sci. U.S.A. 101*, 8858−8863]. To probe the mechanisms of GTPase activation protein (GAP)-facilitated GTP hydrolysis reactions, we measured the $^{18}O$ KIEs in GTP hydrolysis catalyzed by Ras in the presence of $GAP^{334}$ or $NF1^{333}$, the catalytic fragment of p120GAP or NF1. The KIEs in the leaving group oxygens (the $\beta$ nonbridge and the $\beta-\gamma$ bridge oxygens) reveal that chemistry is rate-limiting in $GAP^{334}$-facilitated GTP hydrolysis but only partially rate-limiting in the $NF1^{333}$-facilitated GTP hydrolysis reaction. The KIEs in the $\gamma$ nonbridge oxygens and the leaving group oxygens reveal that the $GAP^{334}$ or $NF1^{333}$-facilitated GTP hydrolysis reaction proceeds through a loose transition state that is similar in nature to the transition state of the GTP hydrolysis catalyzed by Ras alone. However, the KIEs in the pro-S $\beta$, pro-R $\beta$, and $\beta-\gamma$ oxygens suggest that charge increase on the $\beta-\gamma$ bridge oxygen is more prominent in the transition states of $GAP^{334}$- and $NF1^{333}$-facilitated reactions than that catalyzed by the intrinsic GTPase activity of Ras. The charge distribution on the two $\beta$ nonbridge oxygens is also very asymmetric. The catalytic roles of active site residues were inferred from the effect of mutations on the reaction rate and KIEs. Our results suggest that the arginine finger of GAP and amide protons in the P-loop of Ras stabilize the negative charge on the $\beta-\gamma$ bridge oxygen and the pro-S $\beta$ nonbridge oxygen of a loose transition state, whereas Lys-16 of Ras and $Mg^{2+}$ are only involved in substrate binding.

Ras is the prototypical member of the small G protein superfamily that mediates diverse signaling pathways in eukaryotes (*1*, *2*). Like other G proteins, Ras alternates between the guanosine 5′ diphosphate (GDP[1])-bound inactive state and the GTP-bound active state. GTP-bound Ras is capable of binding to different effector proteins and thereby activating multiple signaling pathways. The intrinsic GTPase activity of Ras is very low, necessitating the down-regulation of Ras activity *in vivo* by GTPase activating proteins (GAPs) (*3*), including p120GAP (*4*) and neurofibromin 1(NF1) (*5*). Both GAPs increase the rate of GTP hydrolysis by more than $10^5$-fold, from $10^{-4}$ $s^{-1}$ to at least 8 $s^{-1}$ (*6*, *7*). Mutations in Ras that impair either intrinsic or GAP-facilitated GTPase activity leave Ras in a prolonged state of activation and were found in 30% of cancers (*8*). Mutations in NF1 are responsible for the pathogenesis of neurofibromatosis type 1 (*9*).

The chemical mechanism of Ras-catalyzed GTP hydrolysis, in particular the nature of the transition state in the intrinsic or GAP-facilitated GTPase reaction, has been the focus of considerable debate. The traditional view holds that the hydrolysis of a phosphate monoester with a good leaving group, of which GTP is one example, proceeds through a metaphosphate-like, loose transition state that features extensive cleavage to the bond between the phosphorus and the leaving oxygen but little or no bond formation between the phosphorus and the nucleophile (*10*−*14*). Recent computational studies suggest that metaphosphate is generated as a discrete intermediate in the reaction pathway before it is attacked by the nucleophilic water to generate phosphate (*15*, *16*). An alternative, substrate-assisted, mechanism involves a proton transfer from the attacking water to GTP as a pre-equilibrium step (*17*−*19*). The hydroxide thus formed then attacks the $\gamma$ phosphorus to form a phosphorane intermediate, which decays in the rate-limiting step to generate GDP and phosphate. Resolution of the mechanism is the key to the elucidation of the catalytic roles of the enzyme residues in GTP hydrolysis.

Infrared and Raman spectroscopic measurements clearly revealed that, upon binding to Ras, the $P_\beta-O_{\beta\ \text{nonbridge}}$ bonds of GTP are weakened, but $P_\gamma-O_{\gamma\ \text{nonbridge}}$ bonds are strengthened (*20*−*22*). If the distortion of the electronic structure of GTP

†This project was supported by National Institutes of Health grant GM0714420.

*To whom correspondence should be addressed. Tel: 214-648-9269. Fax: 214-648-3346. E-mail: xinlin.du@utsouthwestern.edu.

[1]Abbreviations: GTP, guanosine 5′ triphosphate; GDP, guanosine 5′ diphosphate; GMP, guanosine 5′ monophosphate; KIE, kinetic isotope effect; GAP, GTPase activation protein; NF1, neurofibromin; IRMS, isotope ratio mass spectrometry.


Published on Web 4/7/2009

by Ras represents destabilization of the ground-state in the direction of the transition state, it can be inferred that the transition state is loose. Indeed, our earlier studies revealed substantial $^{18}O$ KIE in the $\beta-\gamma$ bridge oxygen and $\beta$ nonbridge oxygens in Ras-catalyzed GTP hydrolysis, demonstrating substantial cleavage of $P_\gamma-O_{\beta\gamma\ \text{bridge}}$ and $P_\beta-O_{\beta\ \text{nonbridge}}$ bonds at the transition state (*23*). KIE in the two $\beta$ nonbridge oxygens indicated that charge generated by the cleavage of $P_\gamma-O_{\beta\gamma\ \text{bridge}}$ bond is delocalized into the two $\beta$ nonbridge oxygen atoms through resonance structures. The KIE data, together with the crystal structures of Ras in complex with various GTP analogues (*24*, *25*), provide insight into how Ras catalyzes GTP hydrolysis. Charge increase on the leaving group oxygens, namely, the $\beta-\gamma$ bridge and the two $\beta$ nonbridge oxygens, indicates that the interactions of Ras with the three leaving group oxygen atoms become stronger at the transition state and thereby afford preferential stabilization of the transition state. These interactions are mainly mediated by the P loop of Ras: the amide hydrogen of Gly-13 forms a short hydrogen bond with the $\beta-\gamma$ bridge oxygen; the main chain NH groups of Val-14, Gly-15, and Lys-16, and the side chain of Lys-16 interact with the *pro-S* $\beta$ nonbridge oxygen; the main chain NH of Ser-17 and $Mg^{2+}$ interacts with the *pro-R* $\beta$ oxygen (Figure 1). By contrast, interactions between the $\gamma$ nonbridge oxygens and the $Mg^{2+}$, the main chain NH groups of Thr-35 and Gly-60, and the side chain of Lys-16 are not expected to provide electrostatic stabilization of the transition state over the ground state.

Structural, biochemical, and computational studies led to the notion that GAP$^{334}$ facilitates the GTPase of Ras by stabilizing a catalytically competent conformation of Ras and by providing an arginine residue to electrostatically stabilize the transition state (*13*, *26*−*28*) . The crystal structure of Ras in complex with GAP$^{334}$, a catalytic fragment of p120GAP, and GDP·$AlF_3$, a transition state analogue (Figure 1), revealed that GAP$^{334}$ stabilizes Switch II of Ras in a catalytically competent conformation (*26*). In this conformation, the main chain carbonyl oxygen of Thr-35 of Ras and the side chain oxygen atom of Gln-61 of Ras, which points away from the $\gamma$ phosphoryl group in the absence of GAP$^{334}$, form hydrogen bonds with the nucleophilic water and orient it for inline attack on the $\gamma$ phosphorus. In addition, Arg-789 of GAP$^{334}$, often referred to as the arginine finger, extends into the active site of Ras to interact directly with the $\beta-\gamma$ bridge oxygen and one of the $\gamma$ nonbridge oxygen atoms. The critical role of the arginine finger in catalysis was confirmed by biochemical and computational studies (*27*, *28*). NF1$^{333}$, the catalytic fragment of NF1, is structurally similar to GAP$^{334}$ and also possesses a catalytic arginine finger (*27*, *29*). Therefore, NF1 was proposed to facilitate GTP hydrolysis by a similar mechanism (*29*).

Here, we address the mechanism of GAP-facilitated GTP hydrolysis using $^{18}O$ KIE as a probe of the transition state structures in these reactions. We have synthesized a suite of $^{18}O$-labeled GTP molecules (Figure 2) that allow the determination of the KIEs in the oxygen atoms at or geminal to the scissile bond. The KIE in $\gamma^{18}O_3$-labeling is equivalent to the secondary KIE in the hydrolysis of phosphate monoesters. The charge on the $\beta-\gamma$ bridge oxygen due to the cleavage of $P_\gamma-O_{\beta\gamma\ \text{bridge}}$ bond is delocalized into the two $\beta$ nonbridge oxygens. The electron delocalization effectively increases the bond order of the $\beta-\gamma$ bridge oxygen but decreases the bond order of the two $\beta$ nonbridge oxygen atoms. Therefore, the KIE in $\beta^{18}O_3$, instead of the KIE in the $\beta-\gamma$ bridge oxygen alone, better reflects the extent of cleavage to the $P_\gamma-O_{\beta\gamma\ \text{bridge}}$ at the transition state (*23*). The KIE in the $\beta-\gamma$ bridge oxygen is determined by the ratio of the KIE in $\beta^{18}O_3$ to that in $\beta^{18}O_2$ or by the ratio of KIE in $\gamma^{18}O_4$ to that in $\gamma^{18}O_3$. KIEs in the $\beta-\gamma$ bridge, the pro-S $\beta$, and the pro-R $\beta$ oxygens afford stereospecific probes of changes in bond orders and thereby the changes in the charges on these atoms at

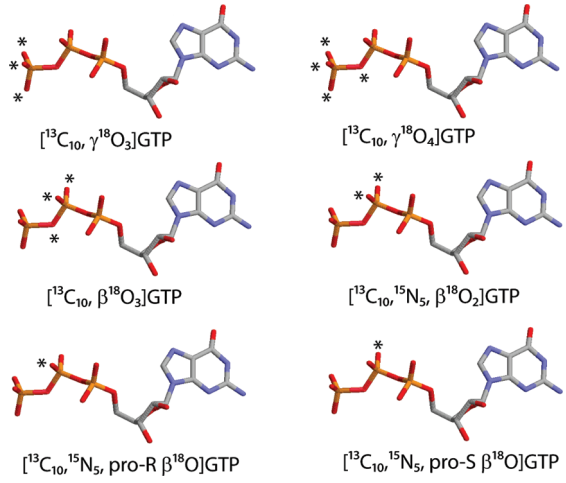


FIGURE 2: Double-labeled nucleotides used in this study. Carbon, nitrogen, oxygen, and phosphorus atoms are colored in silver, blue, yellow, and red, respectively. $^{18}O$-labels are indicated by *.

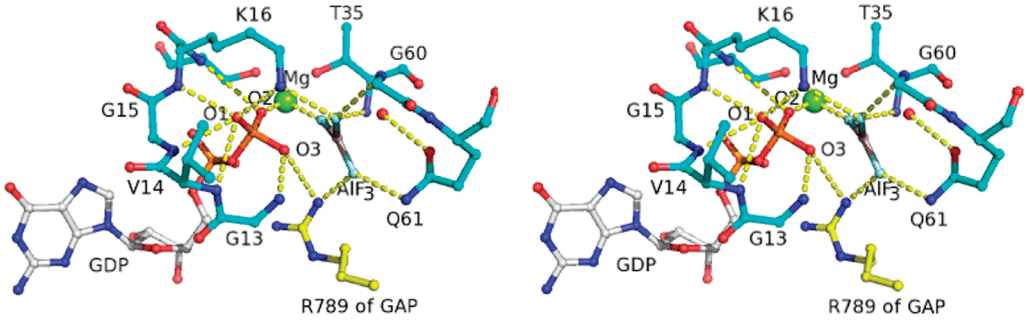


FIGURE 1: Active site of Ras in complex with GAP$^{334}$ and GDP·$AlF_3$, a transition state analogue, in the crystal structure of Ras·GDP·$AlF_3$·RasGAP (PDB ID 1WQ1). O1, O2, and O3 refer to the pro-S $\beta$ nonbridge oxygen, the pro-R $\beta$ nonbridge oxygen, and the $\beta-\gamma$ bridge oxygen, respectively. The functional groups of Ras that contribute to interactions with the pro-S $\beta$ nonbridge oxygen include the main chain NH groups of Val-14, Gly-15, and Lys-16, as well as the N$\zeta$ of Lys-16. The main chain NH of Ser-17 and $Mg^{2+}$ interact with pro-R oxygen. The amide hydrogen of Gly-13 forms a strong hydrogen bond with the $\beta-\gamma$ bridge oxygen. Interactions between Ras and $\gamma$ nonbridge oxygens are realized by $Mg^{2+}$, the main chain NH of Thr-35 and Gly-60, the side chain of Gln-61, and the side chain of Lys-16. Arg-789 of GAP$^{334}$ is positioned to interact with both the $\beta-\gamma$ bridge oxygen and one $\gamma$ nonbridge oxygen.

the transition state. Analysis of the kinetic behavior and KIEs of certain Ras mutants has enabled us to address the roles of the highly conserved residues, Lys-16 and Gln-61, in the catalytic site of Ras. In experiments with an arginine finger mutant of $NF1^{333}$, we have assessed the role of the arginine finger in GAP-facilitated GTP hydrolysis.

## MATERIALS AND METHODS

*Materials*. Guanine nucleotides uniformly labeled with $^{13}C$ or $^{13}C$, $^{15}N$ were purchased from Spectra Gases, Inc. The $^{13}C$ enrichment is better than 99% as determined by electro-spray mass spectrometry. $^{13}C$-depleted GTP ([$^{12}C$]GTP) was either purchased from Spectra Gases or synthesized as described earlier (*30*). The residual carbon isotope ratios in the [$^{12}C$]GTP purchased or synthesized for this study were 0.23% and 0.09%, respectively. $H_2^{18}O$ (97% enriched) was from Isotech. Other reagents for chemical synthesis were obtained from Sigma.

*Synthesis of $^{18}O$,$^{13}C$-labeled nucleotides*. $^{18}O$,$^{13}C$-labeled nucleotides were synthesized by coupling $^{18}O$-labeled phosphate or phosphate to guanine nucleotides uniformly labeled with $^{13}C$. The schemes for the synthesis of the six double-labeled nucleotides, [$^{13}C_{10}$, $\gamma^{18}O_3$]GTP, [$^{13}C_{10}$, $\gamma^{18}O_4$]GTP, [$^{13}C_{10}$, $\beta^{18}O_3$]GTP, [$^{13}C_{10}$,$^{15}N_5$, $\beta^{18}O_2$]GTP, [$^{13}C_{10}$,$^{15}N_5$, pro-S $\beta^{18}$O]GTP, and [$^{13}C_{10}$,$^{15}N_5$, pro-R $\beta^{18}$O] are provided as Supporting Information. The detailed procedures for the synthesis of [$^{13}C_{10}$, $\gamma^{18}O_3$]GTP, [$^{13}C_{10}$, $\gamma^{18}O_4$]GTP, [$^{13}C_{10}$, $\beta^{18}O_3$]GTP, and [$^{13}C_{10}$,$^{15}N_5$, $\beta^{18}O_2$]GTP were described earlier (*23*, *30*). Electrospray mass spectrometry was used to deduce the $^{18}O$ isotopic purity of $^{18}O$- and $^{13}C$-labeled GTP. The $^{18}O$ enrichment level for [$^{13}C_{10}$, $\gamma^{18}O_3$]GTP, [$^{13}C_{10}$, $\gamma^{18}O_4$]GTP, [$^{13}C_{10}$, $\beta^{18}O_3$]GTP, [$^{13}C_{10}$,$^{15}N_5$, $\beta^{18}O_2$]GTP, [$^{13}C_{10}$,$^{15}N_5$, pro-S $\beta^{18}$O]GTP, and [$^{13}C_{10}$,$^{15}N_5$, pro-R $\beta^{18}$O]GTP were 96%, 94%, 96%, 94%, 95%, and 95%, respectively.

*Synthesis of [$^{13}C_{10}$,$^{15}N_5$, pro-S $\beta^{18}O$]GTP, and [$^{13}C_{10}$,$^{15}N_5$, pro-R $\beta^{18}O$]GTP*. The synthesis of [$^{13}C_{10}$,$^{15}N_5$, pro-S $\beta^{18}$O]GTP and [$^{13}C_{10}$,$^{15}N_5$, pro-R $\beta^{18}$O]GTP was carried out following the methods of Fritz Eckstein. R and S diastereomers of GTP$\beta$S were first synthesized (*31*). Sulfur in the R or S diastereomer was then substituted with $^{18}O$ with the reversion of configuration, yielding [$^{13}C_{10}$,$^{15}N_5$, pro-S $\beta^{18}$O]GTP, and [$^{13}C_{10}$,$^{15}N_5$, pro-R $\beta^{18}$O]GTP, respectively (*32*). We used a modification of the protocol described by Connolly, et al. (*32*) to avoid the production of heavily bromated $^{18}O$ GTP, as follows. GTP$\beta$S (1.5 mg) was mixed with 500 $\mu$L of GDP (80 mM) and 100 $\mu$L of dithiothreitol (300 mM), and the solution was dried on a Speedvac. The residue was dissolved in 100 $\mu$L of $H_2^{18}O$ and re-evaporated, and the step was repeated. Finally, the residue was dissolved in 200 $\mu$L of $H_2^{18}O$ and 600 $\mu$L of *N*-bromosuccinimide (100 mM) in dry dioxane. After 5 min at room temperature, 100 $\mu$L of 1-mercaptoethanol was added to the solution. After 2 min, 3 mL of $H_2O$ was added, and the pH was adjusted to approximately 7.0 with 150 $\mu$L of triethylamine. The solution was then loaded onto a 5 mL HiTrap Q (GE Healthcare) column. GDP and GTP were separated by a 20 column volume, 0 to 1 M gradient of ammonium acetate. The fraction containing GTP was collected and further purified on a 1 mL HiTrap Q column. Ammonium acetate was removed afterward by lyophilization.

*Protein Expression and Purification*. A synthetic gene encoding residues 1 to 166 of human H-Ras was subcloned into a pET28 vector (*33*). The catalytic fragments of SOS1 (residues 564−1049) (*34*), mouse Cdc25 (residue 976−1260, $Cdc25^{Mm285}$) (*35*), human NF1 (residue 1197−1528, $NF1^{333}$) (*36*), and human p120GAP (residue 714−1097, $GAP^{334}$) (*6*) were subcloned into pGEX vectors. Mutations in Ras and $NF1^{333}$ were introduced using the QuickChange kit (Stratagene). His-tagged Ras and GST-fused $Cdc25^{Mm285}$ were coexpressed in *E. coli* strain BL21 (DE3) and copurified as a complex through Ni-affinity, glutathione affinity, and ion-exchange column chromatography. Ras(K16A) in complex with $Cdc25^{Mm285}$ was prepared similarly. Unlike other Ras mutants, Ras(Q61H) interacts with $Cdc25^{Mm285}$ only weakly. When His-tagged Ras(Q61H) and GST-fused $Cdc25^{Mm285}$ were coexpressed bacterially, the stoichiometric complex was not obtained following Ni-affinity and glutathione affinity chromatography. Instead, the Ras(Q61H)−SOS1 complex was prepared and used in this study. First, GST-fused SOS1 was retained on Glutathione−Sepharose beads. A tight complex of Ras(Q61H)-SOS1 is formed when excess Ni-affinity purified, His-tagged Ras(Q61H) was loaded onto the column. The complex was eluted with 10 mM glutathione and further purified by ion-exchange column chromatography. $GAP^{334}$, $NF1^{333}$, or $NF1^{333}$(R1276A) was expressed in BL21(DE3) and purified by glutathione affinity and ion-exchange chromatography.

*Steady State Condition for GTP Hydrolysis Catalyzed by Ras*. A typical GTP hydrolysis reaction for Ras was carried out in 40 $\mu$L volume that contained 136 $\mu$M (11.3 mg/mL) Ras·$Cdc25^{Mm285}$ complex, 1 mM GTP, 100 $\mu$M $MgCl_2$, and 50 mM HEPES at pH 7.5. Reactions typically reached 50% completion after 32 h at 22 °C. Aliquots of 13 $\mu$L were taken, placed in a 100 °C heating block for 20 s to denature the proteins, and then frozen at −20 °C before IRMS analysis. The turnover rate for Ras-catalyzed GTP hydrolysis, determined by measurement of the reaction period during which half of the reactant is consumed, was 0.115 $h^{-1}$ and was only one-sixth of the rate determined under single turnover conditions (*20*). Most of the reduction in rate can be ascribed to the inhibitory effect of $Cdc25^{Mm285}$, which is expected to compete effectively with GTP for Ras and secure Ras in the Ras·$Cdc25^{Mm285}$ complex (*37*). GDP also competes with GTP for Ras and product inhibition becomes significant even before the reaction is half-complete. On the basis of these considerations, it is estimated that about 20% to 25% of Ras existed in the Ras·GTP complex, while most of the Ras was in complex with $Cdc25^{Mm285}$ at the beginning of the reaction.

*Steady State Condition for GAP-Facilitated GTP Hydrolysis Reactions*. Reactions in the presence of $GAP^{334}$ were carried out in 30 $\mu$L volumes that contained 48 $\mu$M (4.0 mg/mL) Ras·$Cdc25^{Mm285}$ complex, 0.084 $\mu$M (0.0058 mg/mL) $GAP^{334}$, 1 mM GTP, 25 $\mu$M $MgCl_2$, and 50 mM HEPES at pH 7.5. Typically, a reaction reached 50% completion in 40 min. For other hydrolysis reactions, the same concentration of Ras or Ras mutant in complex with $Cdc25^{Mm285}$ was used and the concentration of GAP was varied. The GAP concentration and the half-time of the reactions were as follows: 17 $\mu$M $GAP^{334}$ and a $t_{1/2}$ of 40 min for Ras(K16A)-$GAP^{334}$; 0.087 $\mu$M $NF1^{333}$ and a $t_{1/2}$ of 60 min for Ras- $NF1^{333}$; 4.3 $\mu$M $NF1^{333}$ and a $t_{1/2}$ of 40 min for Ras (K16A)-$NF1^{333}$; and 17 $\mu$M $NF1^{333}$(R1276A) and a $t_{1/2}$ of 270 min for Ras-$NF1^{333}$(R1276A). A typical experiment for Ras (Q61H)-$NF1^{333}$ was carried out in 30 $\mu$L volume containing 51 $\mu$M (5.5 mg/mL) Ras(Q61H)·SOS1 complex and 67 $\mu$M (4.6 mg/mL) $NF1^{333}$ and reached 30% completion in 240 min. The reactions for Ras-$GAP^{334}$ and Ras-$NF1^{333}$ were carried out in the presence of 25 $\mu$M $MgCl_2$. Other reactions were carried out in the presence of 50 $\mu$M $MgCl_2$.

*Determination of KIEs*. The method used to determine KIEs for GTP hydrolysis has been reported in detail (*30*) and is only briefly described here. An internal competition method was employed using $^{18}O$,$^{13}C$-labeled GTP and $^{13}C$-depleted GTP. The double-labeled GTP is labeled with $^{18}O$ at sites of mechanistic interest and with $^{13}C$ at all carbon positions on the sugar and base of the nucleotide, while the $^{16}O$-nucleotide is depleted of $^{13}C$. The relative abundance of the labeled and unlabeled substrates or products is thereby reflected in the carbon isotope ratio ($^{13}C/^{12}C$) in GTP or GDP, which was measured using a LC-coupled IRMS. A KIE can be calculated from the change in the isotope ratio of the substrate GTP relative to that at the beginning of the reaction ($R_s/R_0$), by the changes in the isotope ratio of the product GDP relative to that when hydrolysis is complete ($R_p/R_0$), or by the difference between the isotope ratios in GDP and GTP (*38*). It was established that in our experimental system, the three methods give equivalent results, but the third method offers the best precision (*30*). Therefore, the changes in carbon isotope ratios of GDP and GTP ($R_p/R_s$) in the course of the reaction were used to calculate KIE according to eq 1. In a few cases, we were not able to accurately measure the isotope ratio of GDP, and the KIEs were calculated according to eq 2. Fractional reaction extent was calculated from mass 44 peak areas of GDP and GTP according to eq 3.

$$KIE = \frac{\ln(1-f)}{\ln \frac{1-f}{1-f+fRp/Rs}} \quad (1)$$

$$KIE = \frac{\ln(1-f)}{\ln[(1-f)R_s/R_0]} \quad (2)$$

$$f = \frac{area(GDP)}{area(GDP) + area(GTP)} \quad (3)$$

## RESULTS

KIEs are reported in Table 1 for GTP hydrolysis catalyzed by Ras and Ras mutants, in the presence or absence of GAP$^{334}$, NF1$^{333}$, or the arginine finger mutant of NF1$^{333}$. In addition to wild type proteins, Ras(K16A), Ras(Q61H), and NF1$^{333}$(R1276A) were employed to probe the kinetic mechanism and the perturbation of the transition state by the indicated mutations. Ras and Ras mutants were purified as complexes with guanine nucleotide exchange factors, Cdc25$^{Mm285}$ or SOS1, for several reasons: first, Ras proteins obtained in this way were free of GDP so that the isotope ratio of hydrolysis product (GDP) was not biased by the presence of residual, unlabeled GDP; second, Cdc25$^{Mm285}$ and SOS1 accelerate GTP release and thereby reduce the external forward commitment for the reaction; third, the exchange factors accelerate product (GDP) release so that the steady state rate is not limited byproduct release; last, active Ras(K16A) can only be obtained when copurified with Cdc25$^{Mm285}$. Six double-labeled nucleotides, [$^{13}C_{10}$, $\gamma^{18}O_3$]GTP, [$^{13}C_{10}$, $\gamma^{18}O_4$]GTP, [$^{13}C_{10}$, $\beta^{18}O_3$]GTP, [$^{13}C_{10}$,$^{15}N_5$, $\beta^{18}O_2$]GTP, [$^{13}C_{10}$,$^{15}N_5$, pro-S $\beta^{18}$O]GTP, and [$^{13}C_{10}$,$^{15}N_5$, pro-R $\beta^{18}$O], were used in this study (Figure 2). KIEs in $^{13}C$-labeling or $^{13}C$,$^{15}N$-labeling were measured directly using $^{13}C$- or $^{13}C$,$^{15}N$-labeled nucleotides. Corrections due to the incomplete $^{13}C$ depletion in $^{12}C$-GTP and incomplete $^{18}O$-labeling in double-labeled GTP for the computation of the KIE in $^{18}O$-labeling were carried out according to the formulation of Hermes et al. (*39*).

## DISCUSSION

*Kinetic Mechanisms and Reaction Rates for GAP-Facilitated GTP Hydrolysis*. The minimal kinetic mechanism for a GAP$^{334}$- or NF1$^{333}$-facilitated GTP hydrolysis reaction can be described by eq 4.

$$\mathrm{Ras} + \mathrm{GTP} \underset{k_{-1}}{\overset{k_1}{\rightleftharpoons}} \mathrm{Ras{\cdot}GTP} \underset{k_{-2}}{\overset{k_2}{\rightleftharpoons}} \mathrm{Ras{\cdot}GTP{\cdot}GAP} \xrightarrow{k_3}$$

$$\mathrm{Ras{\cdot}GDP{\cdot}Pi{\cdot}GAP} \xrightarrow{k_4} \mathrm{Ras{\cdot}GDP} + \mathrm{Pi} + \mathrm{GAP} \quad (4)$$

The reaction may be considered as a system with GAP as the enzyme and Ras·GTP as the substrate. The steady

Table 1: KIEs in GTP Hydrolysis Reactions Catalyzed by Ras, GAP (GAP$^{334}$ or NF1$^{333}$), and Mutants[a]

| labeling | Ras | Ras-GAP$^{334}$ | Ras(K16A)-GAP$^{334}$ | Ras-NF1$^{333}$ | Ras(K16A)-NF1$^{333}$ | Ras(Q61H)-NF1$^{333}$ | Ras-NF1$^{333}$(R1276A) |
|---|---|---|---|---|---|---|---|
| $^{13}C$ | 1.0014 (8, 0.03%) | 1.0049 (11, 0.04%) | 1.0051 (8, 0.06%) | 1.0045 (11, 0.06%) | 1.0039 (20, 0.06%) | 1.0006 (6, 0.17%) | 1.0035 (12, 0.04%) |
| $^{13}C$, $^{15}N$ | 1.0016 (6, 0.06%) | 1.0057 (9, 0.05%) | 1.0060 (15, 0.05%) | 1.0055 (9, 0.04%) | 1.0049 (9, 0.08%) | 1.0007 (6, 0.11%) | 1.0036 (8, 0.03%) |
| $\gamma^{18}O_3$[b] | 0.9994 (6, 0.09%) | 1.0012 (15, 0.11%) | 0.9989 (15, 0.17%) | 0.9992 (9, 0.09%) | 0.9983 (10, 0.08%) | 0.9991 (6, 0.19%) | 0.9994 (9, 0.05%) |
| $\gamma^{18}O_4$[b] | 1.0106 (6, 0.04%) | 1.0172 (15, 0.08%) | 1.0140 (14, 0.14%) | 1.0050 (9, 0.14%) | 1.0030 (6, 0.11%) | 1.0083 (6, 0.19%) | 1.0132 (9, 0.10%) |
| $\beta^{18}O_3$[b] | 1.0192 (5, 0.05%) | 1.0220 (21, 0.14%) | 1.0214 (17, 0.18%) | 1.0077 (17, 0.09%) | 1.0048 (11, 0.08%) | 1.0179 (6, 0.18%) | 1.0202 (9, 0.08%) |
| $\beta^{18}O_2$[c] | 1.0078 (6, 0.08%) | 1.0057 (9, 0.08%) | 1.0051 (9, 0.14%) | 1.0000 (9, 0.10%) | 0.9995 (7, 0.09%) | 1.0096 (6, 0.14%) | 1.0069 (9, 0.05%) |
| pro-S $\beta^{18}$O[c] | 1.0042 (6, 0.07%) | 1.0044 (9, 0.11%) | 1.0039 (9, 0.16%) | 1.0012 (9, 0.11%) | 1.0003 (7, 0.10%) | 1.0046 (6, 0.12%) | 1.0033 (9, 0.08%) |
| pro-R $\beta^{18}$O[c] | 1.0028 (6, 0.07%) | 1.0006 (8, 0.06%) | 1.0010 (8, 0.11%) | 0.9975 (9, 0.06%) | 0.9972 (9, 0.16%) | 1.0062 (6, 0.14%) | 0.9994 (9, 0.06%) |
| $\gamma^{18}O_4/\ \gamma^{18}O_3$[d] | 1.0112 (0.10%) | 1.0160 (0.14%) | 1.0151 (0.21%) | 1.0058 (0.17%) | 1.0047 (0.14%) | 1.0092 (0.27%) | 1.0138 (0.11%) |
| $\beta^{18}O_3/\ \beta^{18}O_2$[e] | 1.0113 (0.09%) | 1.0162 (0.15%) | 1.0162 (0.24%) | 1.0077 (0.13%) | 1.0053 (0.12%) | 1.0082 (0.22%) | 1.0132 (0.09%) |
| $\beta-\gamma$ bridge[f] | 1.0113 | 1.0161 | 1.0157 | 1.0068 | 1.0050 | 1.0087 | 1.0135 |
| rate[g] | 0.115 $h^{-1}$ | 2.5 $s^{-1}$ | 0.012 $s^{-1}$ | 1.6 $s^{-1}$ | 0.048 $s^{-1}$ | 0.00031 $s^{-1}$ | 0.0018 $s^{-1}$ |

[a] Each KIE is an average with the number of determination and associated errors listed in parentheses. The following equation was utilized to correct for the incomplete $^{13}C$-depletion in [$^{12}C$, $^{16}O$]GTP and incomplete $^{18}O$-labeling in double-labeled GTP $^{18}(V/K) = WY/[A - (W - A)[(1 - B)Z/(BX)] - W(1 - Y)]$, where $W$ = the observed isotope effect [KIE in $^{13,18}(V/K)$ or $^{13,15,18}(V/K)$], $A$ = the isotope effect in $^{13}C$- or $^{13}C$,$^{15}N$-labeling, $X$ = the fraction of $^{13}C$ in the double-labeled GTP (0.99), $Y$ = the fraction of $^{18}O$ in double-labeled GTP (0.95), $Z$ = the fraction of $^{13}C$ in the [$^{12}C$, $^{16}O$]GTP (0.23% or 0.09%), and $B$ = the fraction of $^{13}C$- or $^{13}C$,$^{15}N$-labeled GTP in the mixture of reactant (0.89% or 1.03% for Z of 0.23% or 0.09%, respectively). [b] The associated errors for the KIEs in $\gamma^{18}O_3$, $\gamma^{18}O_4$, or $\beta^{18}O_3$ are computed by $\Delta = [(\Delta_1)^2 + (\Delta_2)^2]^{1/2}$, where $\Delta_1$ and $\Delta_2$ are the standard deviations in the corresponding KIEs in $^{13}C$, $^{18}O$-labeling, and $^{13}C$-labeling, respectively. [c] The associated errors for the KIEs in $\beta^{18}O_2$, pro-S $\beta^{18}$O, or pro-R $\beta^{18}$O are computed by $\Delta = [(\Delta_1)^2 + (\Delta_2)^2]^{1/2}$, where $\Delta_1$ and $\Delta_2$ are the standard deviations in the corresponding KIEs in $^{13}C$, $^{13}N$, $^{18}O$-labeling, and $^{13}C$, $^{15}N$-labeling, respectively. [d] The KIE in the $\beta-\gamma$ bridge oxygen was computed as the ratio of the KIE in $\gamma^{18}O_4$ to the KIE in $\gamma^{18}O_3$. [e] The KIE in the $\beta-\gamma$ bridge oxygen was computed as the ratio of the KIE in $\beta^{18}O_3$ to the KIE in $\beta^{18}O_2$. [f] The average of KIEs in the $\beta-\gamma$ bridge oxygen computed in the two ways. [g] The steady state rate for Ras, 0.5 $[GTP]_0/([Ras]xt_{1/2})$; steady state rates for GAP-facilitated reactions, 0.5 $[GTP]_0/([GAP]xt_{1/2})$.

state rate takes the form of Michaelis−Menten equation as in eq 5.

$$v = \frac{k_3[\text{GAP}][\text{Ras}\cdot\text{GTP}]}{K_m + [\text{Ras}\cdot\text{GTP}]} \quad (5)$$

Under saturating or limiting concentration of Ras·GTP, the reaction rate is given by

$$v = k_3[\text{GAP}] \quad (6)$$

or

$$v = (k_3/K_m)[\text{GAP}][\text{Ras}\cdot\text{GTP}] \quad (7)$$

respectively. In a typical experiment with GAP, the concentration of Ras·GTP is estimated to be around 12 $\mu$M (~25% of total Ras; Materials and Methods). The values of $K_m$ for GAP$^{334}$ and NF1$^{333}$ were reported to be 4.8 $\mu$M and 0.13 $\mu$M, respectively (*7*, *27*). Therefore, the steady state rates for GAP$^{334}$-facilitated or NF1$^{333}$-facilitated GTP hydrolysis can be approximated by eq 6.

*Practical Considerations in the Interpretation of KIEs*. A KIE is defined as a ratio of the reaction rate of the substrate containing light isotopes of the atoms of interest to that of the substrate in which the corresponding atoms are substituted by a heavier isotope (*40*). Isotopic substitution lowers the vibrational energy levels of a molecule to an extent that depends on geometry and bond strength. If bond order decreases at the transition state, isotopic substitution lowers the zero point vibrational energy of the ground-state more than that of the transition state, which causes an increase in the activation energy for the heavier molecule and results in a normal isotope effect ($>1$). In the opposite case where the bond order in the transition state increases, the activation energy is lower for the heavier isotopomer, and an inverse isotope effect ($<1$) is observed. If the labeled atoms are involved in reaction coordinates, there is also a normal ($>1$) contribution to the isotope effect from the reaction coordinate. The magnitudes of the KIEs often permit qualitative or quantitative description of the transition state (*41*, *42*).

The KIE observed for an enzyme-catalyzed reaction is a function of both the intrinsic KIE in the chemical step and the rate constants for nonchemical steps such as substrate binding and release, formation of intermediates, and conformational changes (*38*, *43*). For the GAP$^{334}$- or NF1$^{333}$-facilitated GTP hydrolysis reaction as described by eq 4, the observed KIE is an isotope effect in $V/K$ and is given by the following:

$$^{18}(V/K) = \frac{^{18}k_3 + c_f}{1 + c_f} \quad (8)$$

$$c_f = (k_3/k_{-2})(1 + k_2/k_{-1}) \quad (9)$$

Equation 8 predicts that the observed KIEs are reduced, relative to the intrinsic KIEs in the chemical step ($^{18}k_3$), by forward commitment ($c_f$), which is the ratio of the forward rate of the Ras·GTP·GAP complex ($k_3$) to the net rate of GTP release from this complex to the solution. There has been no evidence in the literature for reversible cleavage the $P_\gamma$−$O_{\beta\gamma}$ bond; therefore, a reverse commitment is not considered here. Two terms, $k_3/k_{-2}$ and $1 + k_2/k_{-1}$, contribute to $c_f$. The first term is an internal commitment and relies only on the kinetic properties of the Ras·GTP·GAP complex, whereas the second term depends on the concentrations of Ras·GTP and GAP. In order to maximize the observed KIE, experimental conditions were designed to minimize $1 + k_2/k_{-1}$. First, a guanine nucleotide exchange factor, either Cdc25$^{Mm285}$ or SOS1, was included in the reaction mixture to accelerate GTP release from Ras·GTP ($k_{-1}$). Second, with the exception of very slow reactions, such as the hydrolysis catalyzed by Ras(Q61H)-NF1$^{333}$, only catalytic amounts of GAP were used so that $k_2$ is minimized. For all reactions, the observed KIEs did not change when the concentration of GAP was varied several fold in either direction. Since $k_2$ is expected to depend on the free concentration of GAP, the independence of KIEs on GAP concentration suggests that $1 + k_2/k_{-1}$ is very close to unity and does not significantly contribute to $c_f$.

*Transition State Structure for Ras-Catalyzed GTP Hydrolysis Is Loose*. We previously reported the KIEs in the GTP hydrolysis reaction catalyzed by Ras (*23*). Having improved our analytical method (*30*) and adopted different reaction conditions, we redetermined these KIEs and report the values in Table 1. In contrast to the previous experiments, which were carried out using catalytic amounts of Cdc25$^{Mm285}$ at 37 °C, stoichiometric amounts of Cdc25$^{Mm285}$ were used in the present study and the reactions were carried out at room temperature. Despite these differences in reaction conditions, the KIEs for $\gamma^{18}O_3$-, $\gamma^{18}O_4$-, $\beta^{18}O_3$-, and $\beta^{18}O_2$-labeling are in agreement with previously reported values within experimental errors.

The nature of the transition state structure for a phosphoryl transfer reaction is revealed by the KIEs in the leaving oxygen and in the geminal nonbridge oxygens (*44*, *45*). The comparable quantities for GTP hydrolysis are the KIEs in $\gamma^{18}O_3$- and $\beta^{18}O_3$-labeling, which reflect the changes in bond orders of the three $\gamma$ nonbridge oxygens and the extent of cleavage of the $P_\gamma$−$O_{\beta\gamma}$ bond, respectively. While interpretation of the KIE in the nonbridge oxygens can be complicated by the extent of proton transfer to the $\gamma$ phosphoryl group at the transition state (*46*), the magnitude of the KIE in the leaving group oxygen is generally accepted as a reliable indicator of the nature of the transition state (*44*, *47*). It is estimated by quantum-mechanical calculations that the KIE in $\beta^{18}O_3$ for a dissociative pathway is around 1.03 (York, D., personal communication). The observed KIE of 0.9994 in $\gamma^{18}O_3$-labeling and of 1.0192 in $\beta^{18}O_3$-labeling reveal that the Ras-catalyzed GTP hydrolysis involves a loose transition state (*23*).

The KIE in $\beta^{18}O_2$-labeling is 1.0078, indicating that the $P_\beta$−$O_{\beta\ \text{nonbridge}}$ bonds are weakened in the transition state. This reduction in bond order presumably arises through resonance structures that allow distribution of the charge, which results from cleavage of the $P_\gamma$−$O_{\beta-\gamma}$ bond, onto the two $\beta$ nonbridge oxygens (*23*). The KIEs of 1.0042 in the pro-S oxygen and of 1.0028 in pro-R $\beta$ oxygen suggest that charge increases slightly more on the pro-S $\beta$ oxygen than the pro-R $\beta$ oxygen. Crystal structures reveal that the pro-R $\beta$ oxygen is coordinated to the $Mg^{2+}$ cofactor and the amide proton of Ser-17, whereas the pro-S $\beta$ atom accepts hydrogen bonds from three P-loop amide groups and forms an ion-pair with the P-loop Lys-16. It is quite possible that the electrostatic potential is different at two nonbridge oxygen atoms and that the asymmetry in charge increase may reflect the difference.

*GAP$^{334}$- and NF1$^{333}$-Stimulated GTP Hydrolysis Reactions Also Proceed through Loose Transition States*. The observed KIEs of 1.0012 in $\gamma^{18}O_3$-labeling and 1.0220 for $\beta^{18}O_3$-labeling in GAP$^{334}$-stimulated GTP hydrolysis are similar to the respective KIEs of 0.9994 and 1.0192 in the intrinsic GTPase reaction, indicating that GAP$^{334}$ does not change the structure of the transition state. In addition, the magnitude of KIE in $\beta^{18}O_3$ indicates that the forward commitment is small and

that transition-state formation is still rate-limiting in the GAP$^{334}$-facilitated Ras GTPase reaction.

The KIE in $\beta^{18}O_3$ for Ras-NF1$^{333}$ (1.0077) is much smaller than that for Ras-GAP$^{334}$ (1.0220), which suggests that there is significant forward commitment in the NF1$^{333}$-facilitated GTP hydrolysis. This assessment is consistent with biochemical properties of NF1$^{333}$ reported in the literature. The rate of dissociation of NF1$^{333}$ from Ras·GTP·NF1$^{333}$ ($k_{-2}$) was estimated to be 5.5 $s^{-1}$ (*7*), and the rate of GTP cleavage ($k_3$) stimulated by NF1$^{333}$ was reported to be 5.4 $s^{-1}$ (*27*) or 19.5 $s^{-1}$ (*7*) in two separate studies. These rates predict a $c_f$ ($k_3/k_{-2}$) in the range between 0.93 and 3.5, which, for an intrinsic isotope effect close to 1.02, could lead to an observed KIE in the range of 1.005 to 1.01, consistent with the measured value of 1.0077. If the commitment factor is very small, as is expected for the arginine finger mutant, NF1$^{333}$(R1276A), a much larger KIE (1.0202) is observed. Therefore, the intrinsic KIE in $\beta^{18}O_3$ for Ras-NF1$^{333}$ is probably as large as that for Ras-GAP$^{334}$, and it follows that NF1$^{333}$-facilitated GTP hydrolysis reactions proceed through a loose transition state as well.

*Charge Asymmetry at the pro-S and pro-R β Oxygens Increases in GAP-Facilitated Reactions*. The asymmetry in the KIEs in the pro-S and pro-R $\beta$ oxygens noted for the intrinsic GTPase activity of Ras is amplified in the GAP-facilitated reactions. The KIEs in pro-S $\beta$ oxygen and pro-R $\beta$ oxygen for Ras-GAP$^{334}$ are 1.0044 and 1.0006, respectively, indicating that there is significant increase in the charge on the pro-S oxygen but not on the pro-R $\beta$ oxygen at the transition state. KIEs for Ras-NF1$^{333}$ are 1.0012 and 0.9975 in pro-S $\beta$ and pro-R $\beta$ oxygen, respectively, indicating that there is a decrease rather than an increase of charge on the pro-R $\beta$ oxygen. The inverse nature of the KIE in pro-R $\beta$ oxygen is confirmed by the observation that the KIE in $\beta^{18}O_2$-labeling (1.0000) is less than that in pro-S $\beta$ oxygen alone (1.0012). Note also that the intrinsic KIE in the pro-R $\beta$ oxygen for the Ras-NF1$^{333}$-catalyzed reaction is more inverse than the observed KIE of 0.9975 because of the significant commitment in the reaction. In summary, GAP$^{334}$- and NF1$^{333}$-facilitated GTP hydrolysis reactions share the loose nature of the transition states but not the pattern of charge increase on the pro-S and pro-R $\beta$ oxygens.

*Charge Increases Prominently on the β−γ Bridge Oxygen in GAP-Facilitated Reactions*. Since the charge due to the cleavage of $P_\gamma-O_{\beta\gamma}$ bond at the transition state is shared between the $\beta-\gamma$ bridge oxygen and the two $\beta$ nonbridge oxygens, it is of mechanistic interest to compare the pattern of charge increase on the three oxygens in different reactions. Computational studies on the hydrolysis of methyl triphosphate reveals that the KIE in the $\beta-\gamma$ bridge oxygen likely has significant contribution from the reaction coordinate (York, D., personal communication) for a concerted mechanism. Therefore, the KIE in the $\beta-\gamma$ bridge oxygen overestimates the charge increase on the $\beta-\gamma$ bridge oxygen relative to the charge increase on the two $\beta$ nonbridge oxygens at the transition state of a reaction. Here, we compare the KIEs in reactions catalyzed by Ras and Ras mutants in the presence of wild type and mutant GAPs and infer qualitative differences in charge distribution between these reactions. Contribution to the KIE in the $\beta-\gamma$ bridge oxygen from the reaction coordinate presumably remains the same in different reactions, and the differences in the KIEs are due to changes in bond orders only, which is directly related to charge increase. Indeed, in all cases, an inverse relationship is observed between the magnitude of the KIE in the bridge oxygen and that in $\beta^{18}O_2$, which is consistent with conservation of charge and validates the correlation between change in charge and KIE.

The KIE in the $\beta-\gamma$ bridge oxygen for the GAP$^{334}$-facilitated GTPase reaction is significantly larger (1.0161) than that for the intrinsic GTPase reaction (1.0113) even though the KIEs in $\beta^{18}O_3$-labeling for the two reactions are similar (1.0220 vs 1.0192). Concomitantly, the KIE in $\beta^{18}O_2$-labeling in GAP$^{334}$-facilitated GTP hydrolysis is smaller (1.0057) than that for the intrinsic reaction (1.0078). These data suggest that in GAP$^{334}$-facilitated GTP hydrolysis there is more charge on the $\beta-\gamma$ bridge oxygen and less on the two $\beta$ nonbridge oxygens than in the reaction catalyzed by the intrinsic activity of Ras. Because of the substantial, but imprecisely known, commitment in the NF1$^{333}$-facilitated GTPase reaction, the KIEs for Ras-NF1$^{333}$ cannot be compared directly with those in the reaction catalyzed by Ras alone. However, a concentration of charge on the $\beta-\gamma$ bridge oxygen similar to that seen in the GAP$^{334}$-facilitated GTPase reaction can be deduced by comparing the KIEs in the $\beta-\gamma$ bridge and $\beta$ nonbridge oxygens. A KIE of unity (1.0000) in $\beta^{18}O_2$ for Ras-NF1$^{333}$ indicates that there is no overall charge increase on the two $\beta$ nonbridge oxygens at the transition state. The KIE in the $\beta-\gamma$ bridge (1.0068), however, is very close to the KIE in $\beta^{18}O_3$-labeling (1.0077), indicating that almost all charge increase occurs on the $\beta-\gamma$ bridge oxygen. Thus, in both GAP$^{334}$- and NF1$^{333}$-assisted reactions, charge increases on the $\beta-\gamma$ bridge oxygen at the expense of $\beta$ nonbridge oxygens as compared with the reaction catalyzed by Ras alone. A computational study also showed that GAP$^{334}$ increases electrostatic potential at the bridge oxygen (*28*). The increase was attributed not only to the presence of the positive charge on the arginine finger but also to the conformation of Ras in the crystal structure of Ras·GDP·$AlF_3$:GAP$^{334}$, which was found to exert higher electrostatic potential at the $\beta-\gamma$ bridge oxygen than the conformation of Ras in the crystal structure of Ras·GPPNP (*28*). The KIE data, together with the computational study, indicate that even though GAPs do not change the nature of the transition state, they can change the charge distribution of the transition state.

*The GAP Arginine Finger Stabilizes Charge at the β−γ Bridge Oxygen at the Transition State*. In the crystal structure of Ras·GDP·$AlF_3$:GAP$^{334}$, Arg-789 of GAP$^{334}$ interacts with both the would-be $\beta-\gamma$ bridge oxygen and one of the $\gamma$ nonbridge oxygens. It is generally accepted that the arginine finger of GAP participates in catalysis by stabilizing the transition state. However, without the knowledge of the structure of the transition state, it is not clear whether Arg-789 stabilizes the negative charge on the $\beta-\gamma$ bridge oxygen of a loose transition state (*13*) or the charge on one of the $\gamma$ nonbridge oxygens of a tight (associative-like) transition state.

In agreement with an earlier report, we found that GAP$^{334}$(R789A) stimulates the GTPase of Ras only marginally (*27*). Consequently, it was not possible to measure KIEs for Ras-GAP$^{334}$(R789A) because the GTP hydrolysis due to intrinsic GTPase was significant relative to the overall level of hydrolysis even in the presence of a stoichiometric amount of GAP$^{334}$(R789A). NF1$^{333}$(R1276A) is also a weak GAP but retains sufficient activity for measurement of KIEs (*27*). The KIE of 1.0202 in $\beta^{18}O_3$ for Ras-NF1$^{333}$(R1276A) is much larger than that of 1.0077 for wild type Ras-NF1$^{333}$, which is consistent with a much reduced $c_f$ as a result of the reduced turnover rate ($k_3$). In contrast, the mutation does not cause any change in the KIE in $\gamma^{18}O_3$, which is 0.9994 for Ras-NF1$^{333}$(R1276A) and 0.9992 for

Ras-NF1$^{333}$. This would be expected if there is no change in mechanism because the change in commitment alone is not expected to affect a KIE that is close to unity. Therefore, we can conclude that the mutation of the arginine finger does not change the nature of the transition state of NF1$^{333}$-facilitated GTP hydrolysis. This is in keeping with our finding that wild type GAP$^{334}$ or NF1$^{333}$, with the arginine fingers, does not change the nature of the transition state of GTP hydrolysis catalyzed by Ras alone. A similar finding was made on studies of Yersinia protein tyrosine phosphatase, where mutation of a conserved Arg residue that interacts with the phosphoryl group does not alter the transition state (*47*). Together, these results would seem to argue against the notion that positive charges interacting with the phosphoryl group can change the nature of the transition state of the hydrolysis reaction of phosphate monoesters.

The mutation of Arg-1276 to Ala leads to increases in the KIEs in $\beta$ nonbridge oxygens. Whereas the KIE in $\beta^{18}O_2$ (1.0000) indicates that there is no overall change of charge at the transition state on the two $\beta$ nonbridge oxygens for Ras-NF1$^{333}$, the KIE in $\beta^{18}O_2$ (1.0069) is significant for Ras-NF1$^{333}$(R1276A). Comparison of the KIEs in the $\beta-\gamma$ bridge oxygen can be made only after scaled by the KIEs in $\beta^{18}O_3$ to remove the differences in commitment factors in these two reactions. The comparison of the KIEs in $\beta^{18}O_2$ for Ras-NF1$^{333}$(0.68%/0.77%) and for NF1$^{333}$(R1276A) (1.34%/2.02%) suggests the mutation results in smaller charge increase at the $\beta-\gamma$ bridge oxygen atom at the transition state. These KIEs support the conclusion that Arg-1276 is a determinant of the electrostatic potential at the $\beta-\gamma$ bridge oxygen and the mutation of Arg-1276 to Ala lowers the electrostatic potential at the $\beta-\gamma$ bridge oxygen. The effect of the mutation on the charge distribution on the leaving group oxygens, together with early observation that there is no charge increase on the $\gamma$-nonbridge oxygens, strongly supports the proposal that the arginine finger of GAP facilitates GTPase of Ras by stabilizing the negative charge on the $\beta-\gamma$ bridge oxygen of a loose transition state.

*Lys-16 of Ras Is Involved in Substrate Binding but Not Transition State Stabilization*. Lys-16 is highly conserved in P-loop nucleotide triphosphatases (*48*). In crystal structures of G proteins bound to GTP and GTP analogues, the conserved lysine residue is invariably found to engage in ionic interactions with both the pro-S $\beta$ nonbridge oxygen and one of the $\gamma$ nonbridge oxygens (*24*, *49*, *50*). It was postulated that Lys-16 is involved in stabilizing the negative charge on the pro-S oxygen at a loose transition state (*13*) or the negative charge on the $\gamma$ nonbridge oxygen at a tight transition state (*51*−*53*).

Ras(K16A) has not been heretofore biochemically characterized, probably because it is difficult to express in *E. coli* as active protein. We obtained active Ras(K16A) by coexpression with CDC25$^{Mm285}$. The complex prepared in this way exhibited GTPase activity in the presence of either GAP$^{334}$ or NF1$^{333}$. As expected, the K16A mutation impairs the GAP-facilitated GTPase activity such that roughly 200-fold higher GAP$^{334}$ or 35-fold higher NF1$^{333}$ concentration was needed to achieve a steady state rate comparable to that for wild type Ras with GAP$^{334}$ or NF1$^{333}$, respectively. Rather surprisingly, the mutation of Lys-16 to Ala does not alter the KIEs in $\beta^{18}O_3$, $\beta^{18}O_2$, pro-S $\beta^{18}O$, or pro-R $\beta^{18}O$ in either GAP$^{334}$- or NF1$^{333}$-facilitated GTP hydrolysis. Inspection of eq 5 reveals that a mutation of Ras can impair the steady state rate in three ways: by reducing the turnover rate ($k_3$); by increasing $K_m$ of Ras·GTP for GAP; or by reducing the affinity of Ras for GTP and thereby lowering the concentration of Ras·GTP. The first two possibilities are unlikely. A decrease in $k_3$ or an increase in $k_{-2}$, which is the only realistic way to increase $K_m$, is expected to lower the commitment ($k_3/k_{-2}$) and lead to a significant increase in the observed KIEs. The paradoxical lack of any effect of the Lys-16 mutation on the KIEs despite its impairment of the steady state rate can be explained by the third possibility, that is, the mutation of Lys-16 reduces the affinity of Ras for GTP and therefore effectively reduces the steady state concentration of Ras·GTP. The mutation need not affect the rate of cleavage ($k_3$) or the dissociation of GAP from Ras·GTP ($k_{-2}$), thereby leaving the commitment and KIEs unchanged. This proposal is consistent with the observation that the K16A mutation does not change the KIEs in the pro-S $\beta$, pro-R $\beta$, and the $\beta-\gamma$ bridge oxygens, which suggests that the interaction of Lys-16 with the pro-R $\beta$ oxygen atom is not strong enough to affect charge distribution on the three oxygen atoms at the transition state.

The proposed effect of the K16A mutation on the affinity of Ras for GTP offers a ready explanation for the observation that NF1$^{333}$ is more efficient than GAP$^{334}$ in stimulating the GTPase activity of Ras(K16A), the reverse of the case for wild type Ras (Table 1). As a consequence of weak binding of Ras(K16A) to GTP, the concentration of Ras(K16A)·GTP is likely much lower than $K_m$ for Ras(K16A)-GAP$^{334}$ or Ras(K16A)-NF1$^{333}$. Consequently, the reaction rate depends on $k_3/K_m$ as described by eq 7, instead of $k_3$, as is the case for wild type Ras and GAP. Although $k_3$ is slightly higher for GAP$^{334}$, NF1$^{333}$ is the more effective enzyme toward Ras(K16A) by virtue of its lower $K_m$ (0.1 $\mu$M vs 5 $\mu$M) (*7*, *27*).

Although the mutation of Lys-16 to Ala does not affect the KIEs in $\beta$ oxygens, it does lower the KIEs in $\gamma^{18}O_3$ from 1.0012 for Ras-GAP$^{334}$ to 0.9989 for Ras(K16A)-GAP$^{334}$. A concomitant decrease from 1.0172 to 1.0140 is also observed in the KIEs for [$\gamma^{18}O_4$]GTP, which shares the $^{18}$O-labels at the three $\gamma$ nonbridge oxygen positions with [$\gamma^{18}O_3$]GTP. The decreases of 0.0023 and 0.0032 in these KIEs are statistically significant in light of the observation that differences in KIEs in $\beta^{18}O_3$, $\beta^{18}O_2$, pro-S $\beta^{18}O$, and pro-R $\beta^{18}O$ for Ras-GAP$^{334}$ and Ras(K16A)-GAP$^{334}$ are all less than 0.0006. In an internal competition experiment, the isotope effects on $V/K$ are measured. As discussed above, the K16A mutation does not affect $V$($k_3$) of the reaction. Therefore, the reductions in the KIEs in $\gamma^{18}O_3$ and $\gamma^{18}O_4$ likely reflect a change in the isotope effect in binding of Ras to the $\gamma$ nonbridge oxygens. If so, the KIE data suggest that Lys-16 contributes as much as 0.002 or 0.003 to the isotope effect in binding.

*Mutation of Gln-61 Disrupts the Stabilization of the Leaving Group Oxygens*. Gln-61 of Ras is a highly conserved residue in the G protein superfamily (*54*). Ras proteins mutated at Gln-61 are frequently found in cancers. Such mutations are oncogenic because they impair the intrinsic and GAP-facilitated GTPase activity of Ras, which results in an abnormally prolonged state of effector activation (*8*). The perceived roles of Gln-61 in catalysis have been evolving ever since the crystal structure of Ras was solved. An earlier proposal that Gln-61 is involved in the activation of the water molecule was disputed on the basis that Gln-61 is a weak base (*24*, *51*, *55*, *56*). Mutational and computational studies argue effectively against the proposal that Gln-61 is involved in transition state stabilization (*28*, *56*). The crystal structure of Ras·GDP·$AlF_3$·GAP$^{334}$ complex suggests that Gln-61 aligns the attacking water molecule and the $\gamma$-phosphoryl group with respect to the protein (*26*). In the metaphosphate-as-intermediate model, Gln-61 was proposed to

mediate the proton transfer from the water to the metaphosphate intermediate (*16*, *57*).

To probe its role in catalysis, we mutated Gln-61 to His, an amino acid that still confers weak activity upon Ras in the presence of $NF1^{333}$ (*6*). The virtually identical KIEs of 0.9992 and 0.9991 in $\gamma^{18}O_3$ for Ras-$NF1^{333}$ and Ras(Q61H)-$NF1^{333}$, respectively, argues against the proposed role of Gln-61 as a mediator of proton transfer in the metaphosphate-as-intermediate model. The KIE of 1.0179 in $\beta^{18}O_3$ is much larger than that for wild type Ras and $NF1^{333}$ (1.0077), which is consistent with a much smaller commitment as a result of the smaller turn over rate ($k_3$). Surprisingly, a drastic effect of the mutation was observed on the KIEs in the leaving group oxygens. KIEs in the $\beta-\gamma$ bridge oxygen (1.0087) and in $\beta^{18}O_2$ (1.0096), when compared with those for the corresponding reactions with wild type Ras (1.0068 and 1.0000, respectively), indicate significantly higher charge increases in the two $\beta$ nonbridge oxygens and concomitantly less charge increases on the $\beta-\gamma$ bridge oxygen. The KIE of 1.0046 in pro-S $\beta$ oxygen and 1.0062 in pro-R $\beta$ oxygen suggest that there is greater charge increase on the pro-R $\beta$ oxygen than on the pro-S $\beta$ oxygen, which is a reversal of the pattern observed for Ras-$NF1^{333}$. These results suggest that the Q61H mutation leads to substantial changes in the electrostatic potential at the three leaving oxygens and, in particular, reduces the electrostatic potential at the $\beta-\gamma$ bridge oxygen. This is surprising in light of the observation that Gln-61 does not interact with the leaving group oxygens directly in the crystal structure of Ras·GDP·$AlF_3$:$GAP^{334}$ (*29*). Thus, the KIE data suggest a previously unsuspected role of Gln-61 in organizing features of the active site that are involved in stabilizing the leaving group oxygens. The side chain $NH_2$ group of Gln-61 and the guanidinium moiety of GAP Arg-789 form hydrogen bonds with the same $\gamma$ nonbridge oxygen. In addition, the $NH_2$ group of the Gln-61 side chain also forms a hydrogen bond with the main chain carbonyl group of Arg-789. It is conceivable that the removal of these interactions by the mutation of Gln-61 disrupts the correct positioning of the arginine finger in the active site of Ras and renders this residue unavailable for stabilizing the transition state.

*Roles of Residues of Ras and GAP in Catalysis*. A dominant theme revealed by the KIEs is that the transition state for Ras-catalyzed GTP hydrolysis is loose. This is the case for reactions catalyzed by the intrinsic GTPase activity of Ras as well as $GAP^{334}$- or $NF1^{333}$-facilitated Ras GTPase activity. Likewise, hydrolysis reactions catalyzed by Ras or GAP mutants proceed through similar transition states. The KIEs in $\gamma^{18}O_3$ are close to unity for all of the reactions. The intrinsic KIEs in $\beta^{18}O_3$ for GAP-facilitated GTP hydrolysis are around 1.02. These KIEs are in the range typically observed for the hydrolysis of phosphomonoesters, of which GTP is one example. In accordance with the existing body of evidence, the KIEs are consistent with loose transition states, in which charge is distributed on the $\beta-\gamma$ bridge oxygen and (by resonance effects) the $\beta$-nonbridge oxygen atoms. This charge distribution imposes specific mechanistic requirements on an enzyme that accelerates the reaction by transition state stabilization. Specifically, we expect that interactions that stabilize charge at leaving group oxygens afford preferential stabilization of a loose transition state and are conducive to catalysis. Interactions with the $\gamma$ phosphoryl group, while likely important for aligning the $\gamma$ phosphoryl group, attacking water, and active site residues, do not provide electrostatic stabilization of the transition state. A second theme that arises from this work is that the distribution of charge among the three leaving group oxygens can differ significantly among reactions catalyzed by Ras, Ras mutants, and Ras−GAP complexes, presumably reflecting differences in electrostatic potential at those positions. Below, we discuss the catalytic roles of several active site residues in Ras, including the $Mg^{2+}$ cofactor, and the catalytic arginine finger in Ras GAPs in light of the pattern of charge distribution on the pro-R $\beta$, pro-S $\beta$, and the $\beta-\gamma$ bridge oxygens.

*$Mg^{2+}$ Cofactor*. In general, $Mg^{2+}$ provides electrostatic stabilization of substrate or the transition state in enzymatic reactions as a cofactor. In the structures of G proteins in complex with GTP, $Mg^{2+}$ interacts with the pro-R $\beta$ oxygen and one of the $\gamma$ nonbridge oxygens (*53*, *54*). In the two GAP-facilitated reactions, KIEs in $\gamma^{18}O_3$ are close to unity, whereas KIEs in the pro-R $\beta$ oxygen are either unity or inverse. Thus, KIE data reveals no charge increase on the $\gamma$ nonbridge oxygens or the pro-R $\beta$ oxygen, suggesting that $Mg^{2+}$ does not preferentially stabilize the transition state in GAP-facilitated GTP hydrolysis. Its role in catalysis is likely limited to orientating GTP and neutralizing its negative charge in the ground state.

*Ras Lys-16*. The amine group of the conserved P loop lysine residue interacts with both the pro-S $\beta$ nonbridge oxygen and one of the $\gamma$ nonbridge oxygens (*24*). The mutation of Lys-16 to Ala changes neither forward commitment nor the pattern of charge distribution on the three leaving oxygens in either $GAP^{334}$- or $NF1^{333}$-facilitated GTP hydrolysis, strongly suggesting that Lys-16 is not involved in transition state stabilization. The effect of the mutation on KIEs in $\gamma^{18}O_3$- or $\gamma^{18}O_4$-labeling reveals its role in GTP binding through its interaction with one of the $\gamma$ nonbridge oxygens.

*P-Loop Amides*. The amide proton of Ras Gly-13 forms a short hydrogen bond with the $\beta-\gamma$ bridge oxygen, whereas the amide protons of residues 14, 15, and 16 interact with the pro-S $\beta$ oxygen (*24*). In GTP hydrolysis facilitated by both $GAP^{334}$ and $NF1^{333}$, the KIEs in the $\beta-\gamma$ bridge oxygen and the pro-S $\beta$ nonbridge oxygen are normal and significant (the observed KIEs for Ras-$NF1^{333}$ need to be adjusted for a commitment factor), revealing charge increase on these two oxygen atoms at the transition state. Therefore, the amide protons of residues 13, 14, 15, and 16 are expected to afford preferential stabilization of the $\beta-\gamma$ bridge oxygen and the pro-S $\beta$ nonbridge oxygen at the transition state. The catalytic role of the Gly-13 amide proton was first recognized by Maegley et al. (*13*).

*Ras Gln-61*. Essential to the intrinsic or GAP-facilitated GTPase activity of Ras, Gln-61 has been proposed to align the attacking water with respect to the $\gamma$ phosphoryl group or to mediate proton transfer from the attacking water to the phosphoryl group. The effect of its mutation on the KIEs in the leaving oxygens suggests that Gln-61 is important for maintaining features of the active site that stabilize the charge on the leaving group oxygen, although the mechanism by which it might provide such stabilization is not obvious. It is also possible that histidine substitution in particular is responsible for perturbations in KIE. Perhaps more important, the mutation does not change the KIE in $\gamma^{18}O_3$, which argues against its role as a mediator of proton transfer.

*GAP Arginine Finger*. It is generally accepted that the arginine finger of GAP accelerates GTP hydrolysis by providing an additional level of transition state stabilization (*26*). The KIEs for Ras-$NF1^{333}$ and Ras-$GAP^{334}$ reveal the loose nature of the transition state and the significant charge buildup on the $\beta-\gamma$ bridge oxygen at the transition state. Moreover, the KIEs for Ras-$NF1^{333}$(R1276A) reveal that the mutation of the arginine

finger influences the transition state charge increase on the $\beta-\gamma$ bridge oxygen but not on the $\gamma$ nonbridge oxygen. Overall, these data strongly suggest that the arginine finger facilitates the GTPase activity of Ras by stabilizing the charge on the $\beta-\gamma$ bridge oxygen at the transition state.

## CONCLUSIONS

There is considerable evidence in the literature to support the notion that GAP proteins function by reorganizing the Switch II of Ras and by electrostatically stabilizing the transition state. The allosteric effect of GAP is critical for the correct positioning of the nucleophilic water and is potentially important for the proton transfer from the nucleophilic water to the phosphate product or bulk medium. The results of the experiments presented here define the loose nature of the transition state structures and emphasize the effect of transition state stabilization afforded by GAP. The participation of GAP does not change the nature of the transition state, which remains loose in a GAP-facilitated reaction. However, GAP changes the charge distribution among the three leaving group oxygens at the transition state, suggesting that GAP increases the electrostatic potential at the $\beta-\gamma$ bridge oxygen and the pro-S $\beta$ oxygen positions. In particular, the KIE data provide strong support to the hypothesis that the arginine finger of Ras GAPs stabilizes the charge at the $\beta-\gamma$ bridge oxygen at the transition state.

## ACKNOWLEDGMENT

We thank Dr. Alfred Wittinghofer at Max Planck Institute for providing plasmids of $Cdc25^{Mm285}$, $GAP^{334}$, and $NF1^{333}$, Drs. Robert Gregory and Kurt Furgerson at the Stable Isotope Laboratory, Southern Methodist University for granting access to their MAT252 and providing excellent technical support, Dr. Frantz Eckstein at Max Planck Institute for personal communication on the synthesis of stereospecific S-GTP, Dr. Daniel Herschlag for critically reading the manuscript, and Dr. Darrin York at University of Minnesota for personal communication on the computational study on the hydrolysis of methyltriphosphate. Special thanks go to Reginald Du for proof-reading. The characterization of $^{18}O$-, $^{13}C$-labeled nucleotides by electrospray mass spectrometry was carried out by the Protein Chemistry Technology Center at The University of Texas Southwestern Medical Center.

## SUPPORTING INFORMATION AVAILABLE

The schemes for the synthesis of the double-labeled nucleotides. This material is available free of charge via the Internet at http://pubs.acs.org.

## REFERENCES

1. Bourne, H. R., Sanders, D. A., and McCormick, F. (1990) The GTPase superfamily: a conserved switch for diverse cell functions. *Nature (London) 348*, 125–132.
2. Cox, A. D., and Der, C. J. (2003) The dark side of Ras: regulation of apoptosis. *Oncogene 22*, 8999–9006.
3. Boguski, M. S., and McCormick, F. (1993) Proteins regulating Ras and its relatives. *Nature (London) 366*, 643–654.
4. Trahey, M., and McCormick, F. (1987) A cytoplasmic protein stimulates normal N-ras p21 GTPase, but does not affect oncogenic mutants. *Science 238*, 542–545.
5. Xu, G. F., Lin, B., Tanaka, K., Dunn, D., Wood, D., Gesteland, R., White, R., Weiss, R., and Tamanoi, F. (1990) The catalytic domain of the neurofibromatosis type 1 gene product stimulates ras GTPase and complements ira mutants of *S. cerevisiae*. *Cell 63*, 835–841.
6. Gideon, P., John, J., Frech, M., Lautwein, A., Clark, R., Scheffler, J. E., and Wittinghofer, A. (1992) Mutational and kinetic analyses of the GTPase-activating protein (GAP)-p21 interaction: the C-terminal domain of GAP is not sufficient for full activity. *Mol. Cell. Biol. 12*, 2050–2056.
7. Phillips, R. A., Hunter, J. L., Eccleston, J. F., and Webb, M. R. (2003) The mechanism of Ras GTPase activation by neurofibromin. *Biochemistry 42*, 3956–3965.
8. Bos, J. L. (1989) ras oncogenes in human cancer: a review. *Cancer Res. 49*, 4682–4689.
9. Serra, E., Puig, S., Otero, D., Gaona, A., Kruyer, H., Ars, E., Estivill, X., and Lazaro, C. (1997) Confirmation of a double-hit model for the NF1 gene in benign neurofibromas. *Am. J. Hum. Genet. 61*, 512–519.
10. Benkovic, S. J., and Schray, K. J. (1978) Transition States of Biochemical Processes, in *Transition States of Biochemical Processes* (Grandour, R. D., and Schowen, R., Eds.) pp 493−527, Plenum Press, New York..
11. Thatcher, G., and Kluger, R. (1989) In *Advances in Physical Organic Chemistry* (Bethell, D., Ed.) pp 99−265, Academic Press, New York..
12. Admiraal, S. J., and Herschlag, D. (1995) Mapping the transition state for ATP hydrolysis: implications for enzymatic catalysis. *Chem. Biol. 2*, 729–739.
13. Maegley, K. A., Admiraal, S. J., and Herschlag, D. (1996) Ras-catalyzed hydrolysis of GTP: a new perspective from model studies. *Proc. Natl. Acad. Sci. U.S.A. 93*, 8160–8166.
14. Hengge, A. C. (2002) Isotope effects in the study of phosphoryl and sulfuryl transfer reactions. *Acc. Chem. Res. 35*, 105–112.
15. Grigorenko, B. L., Nemukhin, A. V., Cachau, R. E., Topol, I. A., and Burt, S. K. (2005) Computational study of a transition state analog of phosphoryl transfer in the Ras-RasGAP complex: AlF(x) versus MgF3. *J. Mol. Model. 11*, 503–508.
16. Grigorenko, B. L., Nemukhin, A. V., Shadrina, M. S., Topol, I. A., and Burt, S. K. (2007) Mechanisms of guanosine triphosphate hydrolysis by Ras and Ras-GAP proteins as rationalized by ab initio QM/MM simulations. *Proteins 66*, 456–466.
17. Schweins, T., Geyer, M., Kalbitzer, H. R., Wittinghofer, A., and Warshel, A. (1996) Linear free energy relationships in the intrinsic and GTPase activating protein-stimulated guanosine 5′-triphosphate hydrolysis of p21ras. *Biochemistry 35*, 14225–14231.
18. Schweins, T., Geyer, M., Scheffzek, K., Warshel, A., Kalbitzer, H. R., and Wittinghofer, A. (1995) Substrate-assisted catalysis as a mechanism for GTP hydrolysis of p21ras and other GTP-binding proteins. *Nat. Struct. Biol. 2*, 36–44.
19. Klahn, M., Rosta, E., and Warshel, A. (2006) On the mechanism of hydrolysis of phosphate monoesters dianions in solutions and proteins. *J. Am. Chem. Soc. 128*, 15310–15323.
20. Du, X., Frei, H., and Kim, S. H. (2000) The mechanism of GTP hydrolysis by Ras probed by Fourier transform infrared spectroscopy. *J. Biol. Chem. 275*, 8492–8500.
21. Allin, C., and Gerwert, K. (2001) Ras catalyzes GTP hydrolysis by shifting negative charges from gamma- to beta-phosphate as revealed by time-resolved FTIR difference spectroscopy. *Biochemistry 40*, 3037–3046.
22. Cheng, H., Sukal, S., Deng, H., Leyh, T. S., and Callender, R. (2001) Vibrational structure of GDP and GTP bound to RAS: an isotope-edited FTIR study. *Biochemistry 40*, 4035–4043.
23. Du, X., Black, G. E., Lecchi, P., Abramson, F. P., and Sprang, S. R. (2004) Kinetic isotope effects in Ras-catalyzed GTP hydrolysis: evidence for a loose transition state. *Proc. Natl. Acad. Sci. U.S.A. 101*, 8858–8863.
24. Pai, E. F., Krengel, U., Petsko, G. A., Goody, R. S., Kabsch, W., and Wittinghofer, A. (1990) Refined crystal structure of the triphosphate conformation of H-ras p21 at 1.35 A resolution: implications for the mechanism of GTP hydrolysis. *EMBO J. 9*, 2351–2359.
25. Milburn, M. V., Tong, L., deVos, A. M., Brunger, A., Yamaizumi, Z., Nishimura, S., and Kim, S. H. (1990) Molecular switch for signal transduction: structural differences between active and inactive forms of protooncogenic ras proteins. *Science 247*, 939–945.
26. Scheffzek, K., Ahmadian, M. R., Kabsch, W., Wiesmuller, L., Lautwein, A., Schmitz, F., and Wittinghofer, A. (1997) The Ras-RasGAP complex: structural basis for GTPase activation and its loss in oncogenic Ras mutants. *Science 277*, 333–338.
27. Ahmadian, M. R., Stege, P., Scheffzek, K., and Wittinghofer, A. (1997) Confirmation of the arginine-finger hypothesis for the GAP-stimulated GTP-hydrolysis reaction of Ras. *Nat. Struct. Biol. 4*, 686–689.
28. Glennon, T. M., Villa, J., and Warshel, A. (2000) How does GAP catalyze the GTPase reaction of Ras? A computer simulation study. *Biochemistry 39*, 9641–9651.

29. Scheffzek, K., Ahmadian, M. R., Wiesmuller, L., Kabsch, W., Stege, P., Schmitz, F., and Wittinghofer, A. (1998) Structural analysis of the GAP-related domain from neurofibromin and its implications. *EMBO J. 17*, 4313–4327.
30. Du, X., Ferguson, K., Gregory, R., and Sprang, S. R. (2008) A method to determine $^{18}O$ kinetic isotope effects in the hydrolysis of nucleotide triphosphates. *Anal. Biochem. 372*, 213–221.
31. Connolly, B. A., Romaniuk, P. J., and Eckstein, F. (1982) Synthesis and characterization of diastereomers of guanosine 5′-O-(1-thiotriphosphate) and guanosine 5′-O-(2-thiotriphosphate). *Biochemistry 21*, 1983–1989.
32. Connolly, B. A., Eckstein, F., and Fuldner, H. H. (1982) Streospecific substitution of oxygen-18 for sulfur in nucleoside phosphorothioates. *J. Biol. Chem. 257*, 3382–3384.
33. Miura, K., Inoue, Y., Nakamori, H., Iwai, S., Ohtsuka, E., Ikehara, M., Noguchi, S., and Nishimura, S. (1986) Synthesis and expression of a synthetic gene for the activated human c-Ha-ras protein. *Jpn J. Cancer Res. 77*, 45–51.
34. Boriack-Sjodin, P. A., Margarit, S. M., Bar-Sagi, D., and Kuriyan, J. (1998) The structural basis of the activation of Ras by Sos. *Nature (London) 394*, 337–343.
35. Jacquet, E., Baouz, S., and Parmeggiani, A. (1995) Characterization of mammalian C-CDC25Mm exchange factor and kinetic properties of the exchange reaction intermediate p21.C-CDC25Mm. *Biochemistry 34*, 12347–12354.
36. Wiesmuller, L., and Wittinghofer, A. (1992) Expression of the GTPase activating domain of the neurofibromatosis type 1 (NF1) gene in *Escherichia coli* and role of the conserved lysine residue. *J. Biol. Chem. 267*, 10207–10210.
37. Lenzen, C., Cool, R. H., and Wittinghofer, A. (1995) Analysis of intrinsic and CDC25-stimulated guanine nucleotide exchange of p21ras-nucleotide complexes by fluorescence measurements. *Methods Enzymol. 255*, 95–109.
38. Cleland, W. W. (1982) Use of isotope effects to elucidate enzyme mechanisms. *CRC Crit. Rev. Biochem. 13*, 385–428.
39. Hermes, J. D., Morrical, S. W., O'Leary, M. H., and Cleland, W. W. (1984) Variation of Transition-state structure as a function of the nucleotide in reaction catalyzed by dehydrogenase. 2. Formate dehydrogenase. *Biochemistry 23*, 5479–5488.
40. Melander, L., and Saunders, W. H. (1980) *Reaction Rates of Isotopic Molecules*, John Wiley & Sons, New York..
41. Cleland, W. W. (1995) Isotope effects: determination of enzyme transition state structure. *Methods Enzymol. 249*, 341–373.
42. Schramm, V. L., Horenstein, B. A., and Kline, P. C. (1994) Transition state analysis and inhibitor design for enzymatic reactions. *J. Biol. Chem. 269*, 18259–18262.
43. Northrop, D. B. (1981) The expression of isotope effects on enzyme-catalyzed reactions. *Annu. Rev. Biochem. 50*, 103–131.
44. Cleland, W. W., and Hengge, A. C. (1995) Mechanisms of phosphoryl and acyl transfer. *FASEB J. 9*, 1585–1594.
45. Cleland, W. W., and Hengge, A. C. (2006) Enzymatic mechanisms of phosphate and sulfate transfer. *Chem. Rev. 106*, 3252–3278.
46. Aqvist, J., Kolmodin, K., Florian, J., and Warshel, A. (1999) Mechanistic alternatives in phosphate monoester hydrolysis: what conclusions can be drawn from available experimental data?. *Chem. Biol. 6*, R71–80.
47. Hoff, R. H., Wu, L., Zhou, B., Zhang, Z. Y., and Hengge, A. C. (1999) Does positive charge at the active sites of phosphatases cause a change in mechanism? The effect of the conserved arginine on the transition state for phosphoryl transfer in the protein-tyrosine phosphatase from Yersinia. *J. Am. Chem. Soc. 121*, 9514–9521.
48. Leipe, D. D., Koonin, E. V., and Aravind, L. (2003) Evolution and classification of P-loop kinases and related proteins. *J. Mol. Biol. 333*, 781–815.
49. Coleman, D. E., Berghuis, A. M., Lee, E., Linder, M. E., Gilman, A. G., and Sprang, S. R. (1994) Structures of active conformations of Gi alpha 1 and the mechanism of GTP hydrolysis. *Science 265*, 1405–1412.
50. Noel, J. P., Hamm, H. E., and Sigler, P. B. (1993) The 2.2 A crystal structure of transducin-alpha complexed with GTP gamma S. *Nature (London) 366*, 654–663.
51. Prive, G. G., Milburn, M. V., Tong, L., de Vos, A. M., Yamaizumi, Z., Nishimura, S., and Kim, S. H. (1992) X-ray crystal structures of transforming p21 ras mutants suggest a transition-state stabilization mechanism for GTP hydrolysis. *Proc. Natl. Acad. Sci. U.S.A. 89*, 3649–3653.
52. Schlichting, I., Almo, S. C., Rapp, G., Wilson, K., Petratos, K., Lentfer, A., Wittinghofer, A., Kabsch, W., Pai, E. F., and Petsko, G. A..; et al. (1990) Time-resolved X-ray crystallographic study of the conformational change in Ha-Ras p21 protein on GTP hydrolysis. *Nature (London) 345*, 309–315.
53. Wittinghofer, A., and Pai, E. F. (1991) The structure of Ras protein: a model for a universal molecular switch. *Trends Biochem. Sci. 16*, 382–387.
54. Sprang, S. R. (1997) G protein mechanisms: insights from structural analysis. *Annu. Rev. Biochem. 66*, 639–678.
55. Foley, C. K., Pedersen, L. G., Charifson, P. S., Darden, T. A., Wittinghofer, A., Pai, E. F., and Anderson, M. W. (1992) Simulation of the solution structure of the H-ras p21-GTP complex. *Biochemistry 31*, 4951–4959.
56. Chung, H. H., Benson, D. R., and Schultz, P. G. (1993) Probing the structure and mechanism of Ras protein with an expanded genetic code. *Science 259*, 806–809.
57. Grigorenko, B. L., Nemukhin, A. V., Topol, I. A., Cachau, R. E., and Burt, S. K. (2005) QM/MM modeling the Ras-GAP catalyzed hydrolysis of guanosine triphosphate. *Proteins 60*, 495–503.